High-field orientational magnetic phase diagrams of the mixed holmium–yttrium iron garnet $Ho_{0.43}Y_{2.57}Fe_5O_{12}$

2008 J. Phys.: Condens. Matter 20 295231

(http://iopscience.iop.org/0953-8984/20/29/295231)

J. Phys.: Condens. Matter **20** (2008) 295231 (7pp) doi:10.1088/0953-8984/20/29/295231

High-field orientational magnetic phase diagrams of the mixed holmium–yttrium iron garnet $Ho_{0.43}Y_{2.57}Fe_5O_{12}$

A Bouguerra[1,2,5], G Fillion[1], S de Brion[3], S Khène[4], P Wolfers[1] and E K Hlil[1]

[1] Institut Néel, CNRS-UJF, 38042 Grenoble cedex 9, France
[2] Institut des Sciences, Université de Souk-Ahras, 41000 Souk-Ahras, Algeria
[3] GHMFL, CNRS-UJF, 38042 Grenoble cedex 9, France
[4] Département de Physique, Université Badji Mohktar, 23000 Annaba, Algeria

E-mail: abouguerra@gmail.com

Received 11 March 2008, in final form 11 June 2008
Published 1 July 2008
Online at stacks.iop.org/JPhysCM/20/295231

Abstract

H–T magnetic phase diagrams of the $Ho_{0.43}Y_{2.57}Fe_5O_{12}$ garnet, due to spin-reorientation transitions, have been determined in the low temperature range (2–30 K) by magnetization measurement under high static magnetic fields (23 T) on [111] and [110] oriented single crystals. It is shown that a very good agreement between computed and observed phase diagrams can be achieved when the free energy is calculated by direct diagonalization of a Hamiltonian including the crystal field (CF) and the exchange interactions considered in the mean-field formalism.

(Some figures in this article are in colour only in the electronic version)

1. Introduction

The rare-earth iron garnets (REIG) are oxide crystals with cubic structure (space group $Ia\bar{3}d$-(O_h^{10}), no. 230). They are commonly written as $\{R_3^{3+}\}[Fe_2^{3+}](Fe_3^{3+})O_{12}$ (where R denotes a rare-earth element or yttrium) with eight of these formula units per unit cell. The oxygen anions O^{2-}, in general positions 96h (x, y, z), define three types of interstices over which the distribution of the cations is well fixed. These are specified by { }, [ ] and ( ), which refer to 24c (dodecahedral), 16a (octahedral) and 24d (tetrahedral), respectively. All the interactions are negative, and the strong negative superexchange interactions between the spins of Fe^{3+} [a] and Fe^{3+} (d), determine the Néel temperature ($T_N \sim 560$ K) for all REIGs.

Numerous studies have been dedicated to the high-field magnetic transitions in the ferrimagnetic mixed holmium–yttrium iron garnet $Ho_xY_{3-x}Fe_5O_{12}$ ($x < 0.8$) compounds [1–11]. Most of them were carried out under high pulsed magnetic fields [1–9]. The major motivation was to get accurate estimates of the parameters underlying the mechanism of the most interesting behavior of these compounds, namely the discontinuous field-induced transitions which occur below some critical temperature T^*, depending on the concentration x. Indeed, in these compounds, under external magnetic fields, the competing effects of a large exchange interaction with a large crystal-field interaction result in phase diagrams whose transition lines are directly connected to energy levels of the trivalent holmium ion, in other words, to exchange and crystal-field parameters.

The garnet unit cell contains 12 distinct rare-earth {c} sites; six inequivalent ones need be considered because of calculus invariance with inversion (see section 3). At each of these dodecahedral sites, the local symmetry is only D_2 and the Ho^{3+} magnetic moment becomes strongly anisotropic at low temperatures, causing the actual magnetic structure to deviate from Néel's collinear ferrimagnetic model: the six magnetic moments of the rare-earth sublattices form a double-umbrella-shaped structure with the resultant moment M_{Ho} directed along the easy axis ⟨111⟩ and antiparallel to the resultant moment of the iron sublattice [12–14] (see figure 3). The iron resulting moment M_{Fe} is equal to the difference of

[5] Author to whom any correspondence should be addressed (preferably via e-mail or second affiliation address).

moments between [a] and (d) sites occupied by Fe^{3+} cations. In fields $\lessapprox$50 T, it can be considered as the moment of only one rigid sublattice which behaves like yttrium iron garnet (YIG, $x = 0$). For $x < 0.8$, there is no compensation point [1] because $M_{Ho} < M_{Fe}$ is always satisfied. At $T = 4$ K, with increasing field strength, the magnetization curves exhibit jumps [11] corresponding to the passage from a spontaneous ferrimagnetic configuration to a saturated ferromagnetic one, via several canted phases separated by phase transitions of spin-reorientation type. These transitions are rather sharp and step-like, due to the anisotropy of the Ho^{3+} moments which is so huge that they can only flip on a fixed direction related to their local environment; they can therefore be described to a first approximation by a model of an Ising ion whose magnetization direction is along the local z-axis of each rare-earth site (i.e. the Ho moments are strongly fixed to the fourfold axes ⟨001⟩). This means that the six rare-earth sites become two-by-two equivalent and one may consider only three Ho^{3+} sublattices. For a given magnetic field direction, a number of distinct phases, differing in the orientation of the resultant of Ho moments with respect to the applied field, can be stabilized successively when the field is increased, and then, at low temperature, magnetization jumps are observed, corresponding to the successive reversal of the three magnetic moments of the Ho^{3+} sublattices. When the magnetic field is applied along [111], the maximum number of possible phases is four, giving a total of three transitions between them. For [110] and [001] directions, these numbers are reduced by one and two, respectively. At $T = 0$ K, the three Ho moments are equal, implying that during these discontinuous transitions M_{Ho} jumps from one type of ⟨111⟩ direction to another, with simultaneous and appropriate change in M_{Fe} orientation. This model has been useful for a qualitative description of the different orientational phases and the transitions involved between them in such diluted rare-earth compounds, but it does not account quantitatively for all the observations [4, 5, 10, 11]. In particular, when the temperature is raised the observed magnetic transitions become smoother and smoother and vanish all together more quickly at a critical temperature T^* (=18.9 K, present work). In our previous work [11] we showed that any model based on an effective-spin Hamiltonian (ESH) for the Ho^{3+} ions does not sufficiently improve the agreement for the magnetization curves at 4 K.

The present paper is a natural continuation of previously published results [11]. In order to build the phase diagrams of $Ho_{0.43}Y_{2.57}Fe_5O_{12}$ single crystals at $\boldsymbol{H} \parallel [111]$ and $\boldsymbol{H} \parallel [110]$, we have undertaken precise magnetization measurements under high static magnetic fields up to 23 T over the temperature range from 2 to 30 K. The computed free energies (i.e. H–T phase diagrams) and magnetization curves are found comparatively by the ESH technique and by the direct diagonalization of a Hamiltonian including crystal-field (CF) and exchange interactions in a mean-field approximation. The latter is made possible by using an available set of CF parameters, previously determined by Nekvasil [15], without any adjustments. The results will be discussed and compared with experimental data.

2. Experiment

The magnetization measurements were made by the extraction method in static magnetic fields up to 23 T, on the same single crystals of $Ho_{0.43}Y_{2.57}Fe_5O_{12}$ as in [11], where the samples and the experimental methods were explicitly described. The magnetization results are reported in Bohr magnetons per $Ho_{0.43}Y_{2.57}Fe_5O_{12}$ formula unit and the magnetic field H is the applied one. As expected, for an applied field along ⟨111⟩ and ⟨110⟩ directions, the experimental magnetization curves show three and two rather sharp jumps, respectively, which are smeared out and diminish when the temperature is increased and disappear on reaching a critical temperature $T^* = 18.9$ K for the two directions. The maximum abrupt change of the magnetization occurs at the lowest temperatures. The magnetization curve recorded at $T = 4.2$ K when the field is applied along ⟨111⟩ is given in figure 8. The transition fields are well determined by the anomalies on differentiated magnetizations curves with respect to field. The temperature dependence of these fields is shown in figures 5 and 6.

3. Crystal-field calculation

To calculate the energy levels of Ho^{3+} in D_2-symmetry, one can use the general approach with the irreducible tensor-operator technique developed by Racah [16, 17]. In single-particle crystal-field theory, the Hamiltonian in Wybourne's form may be written as [18–20]:

$$\mathcal{H}_{CF} = \sum_{k,q>0,i} B_q^k (C_q^{(k)}(i) + (-1)^q C_{-q}^{(k)}(i)) + \sum_{k,i} B_0^k C_0^{(k)}(i) \tag{1}$$

where $C_q^{(k)}(i)$ is a spherical tensor of rank k depending on the coordinates of the ith electron and the summation involving i is over all f electrons of the ion of the interest; the values of k and q for which the parameters B_q^k are nonzero depend on the site symmetry. The geometrical point symmetry of rare-earth sites is D_2, but the CF effective symmetry always contains the inversion [19, 21], and thus the effective symmetry is D_{2h}, giving rise to nine independent CF parameters ($k = 2, 4, 6$; $q = 0, 2, 4, 6$; $q \leqslant k$). All the CF parameters are real quantities.

For HoGG, the present state of the available optical data prevents us from determining the parameters by fitting. We have used the only set of parameters published so far. These CF parameters were obtained by Nekvasil [15] by interpolating the CF parameters appropriate to Dy^{3+}:YGG [22] and ErGG [23]. So we take for Ho^{3+}:YIG the CF parameters pertaining to Ho^{3+}:YGG, because the cell parameters of YIG and YGG are almost identical. These values of CF parameters (table 1) correspond to D_2-symmetry local axes used by Hutching and Wolf [24]. The local axes ($O\xi$, $O\eta$, $O\zeta$) of the six magnetically inequivalent rare-earth sites used in the calculations, and their relation with those of the crystal cubic unit cell, are shown in figure 1. In this convention, $O\xi$ lies along a ⟨001⟩ direction and the quantization axis $O\zeta$ is chosen to be in ⟨110⟩, which is the fourfold direction of the local pseudocube of eight oxygens surrounding each rare-earth ion.

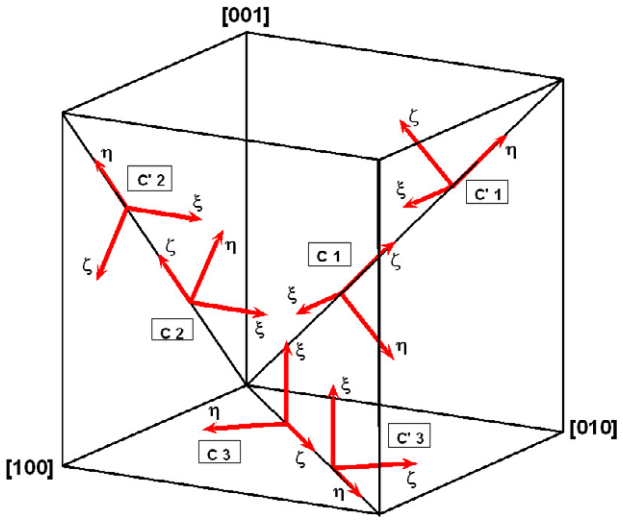

Figure 1. Orientation of orthorhombic local axes ($O\xi$, $O\eta$, $O\zeta$) relative to cubic crystal axes at the six rare-earth sites. One axis lies along a ⟨001⟩ direction and the other two lie along a suitable ⟨110⟩ direction.

Table 1. Crystal-field parameters for Ho^{3+}:YGG [15].

	B_0^2	B_2^2	B_0^4	B_2^4	B_4^4	B_0^6	B_2^6	B_4^6	B_6^6
$(cm^{-1})^a$	−16	94	−2092	270	924	544	−123	973	−57
$(K)^a$	−23	135	−3010	389	1330	783	−177	1400	−82
$(K)^b$	−12	166	−376	307	1390	49	−113	982	−78

[a] Wybourne normalization.
[b] Stevens normalization.

Low-lying levels are nearly pure Russell–Saunders states (i.e. intermediate coupling is negligible), and the first excited multiplet is situated at about 5200 cm^{-1} (7500 K), far from the fundamental multiplet $^5I_8$ [25]. In *LS* coupling scheme, we have diagonalized the crystal-field Hamiltonian both within the ground multiplet states and, to take account of *J*-mixing, in the space of the first three multiplets, namely $^5I_8$, $^5I_7$ and $^5I_6$. The values of intermediate coupled and *LS* coupled reduced matrix elements are given in table 3.2 of [19]. The spin–orbit constant λ has been deduced from the energy splitting between the two first multiplets tabulated by Osborn *et al* [26]. The value taken in this study is $\lambda = -908$ K (-631 cm^{-1}). The results of these calculations are displayed and compared with the experimental energy levels from absorption and emission optical spectra of Ho^{3+}:YGG [27] in figure 2. Not only there is no significant difference for ground multiplet first levels (especially bellow 150 K) in one- and three-multiplet calculations, but they are in excellent agreement with those reported by Nekvasil [15], which involve intermediate coupling. The ground state is a pair of two close singlets Γ_2–Γ_3, separated by about 5 cm^{-1} (7 K). The nearest excited level being about 25 cm^{-1} (36 K) away from it, in agreement with the specific heat measurement of Onn *et al* [28] and our inelastic neutron scattering data [29]. Optical data differ by the non-D_2 symmetry level at 8 cm^{-1} (11.5 K). Consequently, for our purposes and in our experimental range of temperature, we can therefore consider the action of the CF interaction as a perturbation on the free ion ground multiplet $^5I_8$ and use the results of calculations within the multiplet states in an *LS* coupling scheme. The Hamiltonian (1) removes completely the degeneracy of the ground-state multiplet $^5I_8$ and splits the *J* manifold into 17 singlet levels described by the four Γ_i irreducible representations of the D_2 group, namely $5\Gamma_1 \oplus 4\Gamma_2 \oplus 4\Gamma_3 \oplus 4\Gamma_4$.

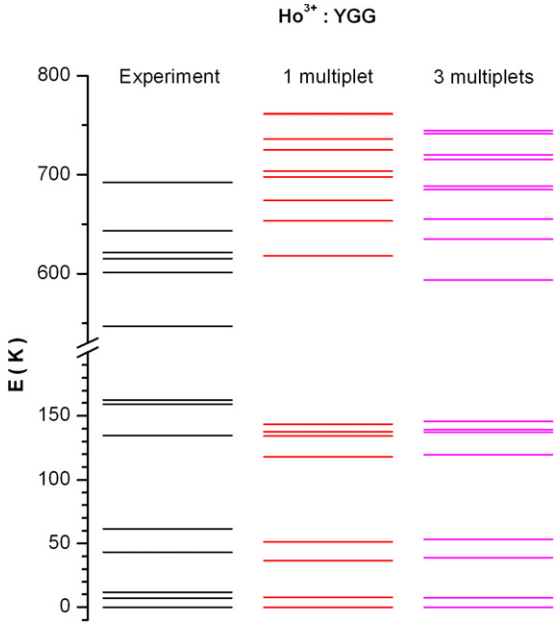

Figure 2. Energy levels of the ground-state multiplet $^5I_8$. We report the results of our one- and three-multiplet calculations together with the splitting from optical measurements [27] (to allow comparison, the calculated ground level is assumed to be zero). The presence of a third level at 8 cm^{-1} (11.5 K) on the optical data is questionable; this level might not come from Ho^{3+} located on a site with D_2 symmetry as was assumed by Nekvasil [15].

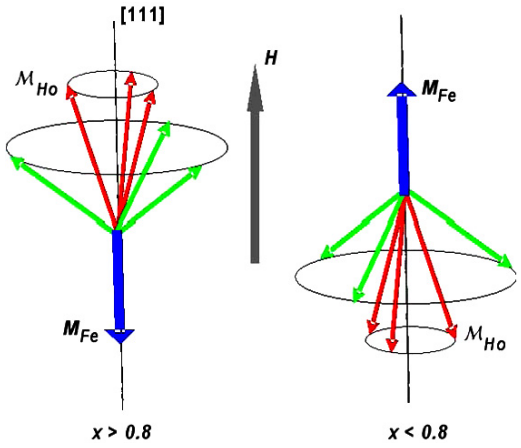

Figure 3. Schematic representation of the arrangement of the initial non-collinear ferrimagnetic structure in the mixed garnet $Ho_xY_{3-x}Fe_5O_{12}$, with respect to the magnetic field direction (case of $\boldsymbol{H} \parallel [111]$). The effective field acting on Ho with moments $\mathcal{M}_{Ho}$ form a double-umbrella structure, increases with *H* when $x > 0.8$ and decreases when $x < 0.8$. The value $x \sim 0.8$ is the concentration for which the spontaneous magnetization of the sample cancels at $T = 0$ K.

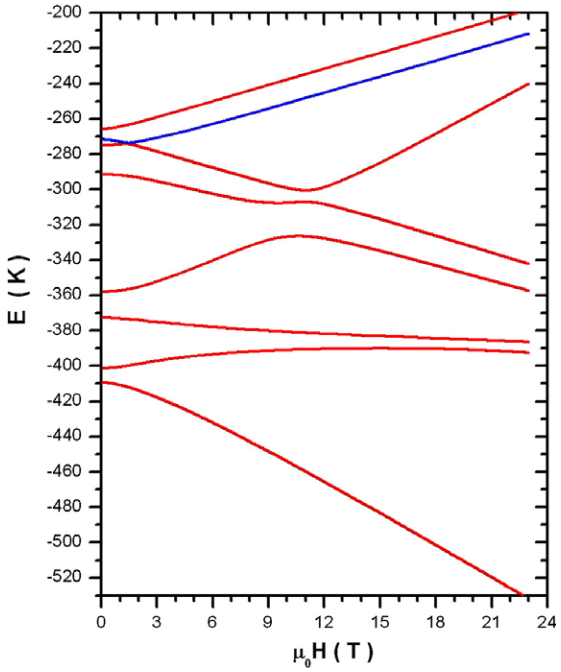

Figure 4. Variation of the first eight energy levels for Ho^{3+}:YGG, at C_i $(i = 1, 2, 3)$ sites as a function of an applied magnetic field. The magnetic field is directed along the crystal threefold axis, $\boldsymbol{H} \parallel [111]$. Note that, when considering Ho^{3+} in YIG, one should think of H as representing the effective field, i.e. the exchange field minus the applied magnetic field ($x < 0.8$).

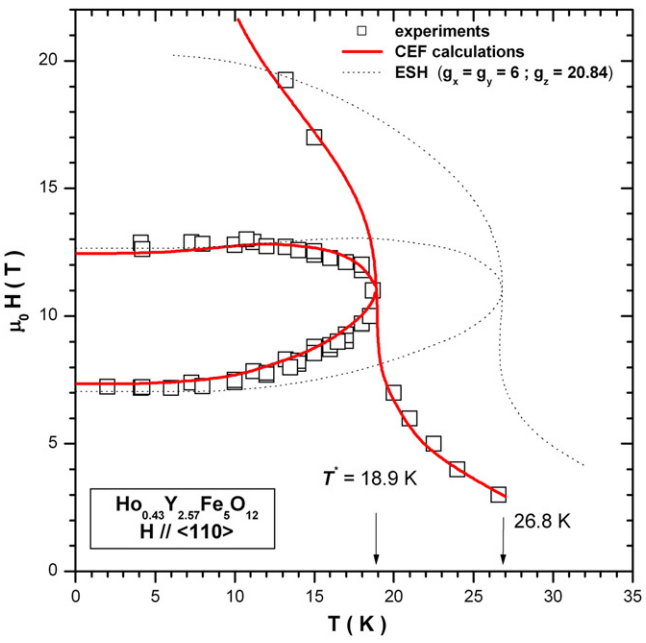

Figure 5. Experimental phase diagram compared with those calculated from crystal-field and effective-spin Hamiltonians: $\boldsymbol{H} \parallel [110]$.

These energy levels and the associated eigenstates depend strongly on the applied magnetic field and its direction. The variation of the low-lying levels versus the magnitude of the magnetic field, in the case of $\boldsymbol{H} \parallel [111]$, is shown in figure 4.

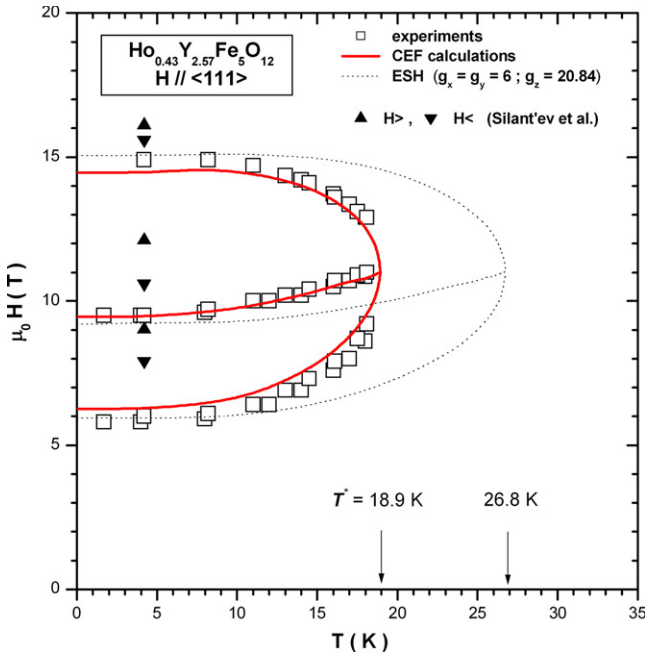

Figure 6. Experimental phase diagram compared with those calculated from crystal-field and effective-spin Hamiltonians: $\boldsymbol{H} \parallel [111]$.

We performed the numerical calculations for Ho^{3+} ions at C_i $(i = 1, 2, 3)$ sites, in Scilab [30] on a PC. In the mixed holmium–yttrium iron garnet with a low concentration of holmium ($x < 0.8$), the resultant moment of the rare-earth sublattice M_{Ho} is smaller than the iron sublattice one, M_{Fe}. Then the applied magnetic field is directed opposite to iron sublattice exchange field acting on Ho^{3+} non-Kramers ion, and the effect of its increasing is to reduce the gap between the ground quasi-doublet levels produced by the exchange field (see figures 3 and 4), pushing the system to (near) degeneracy. To avoid this situation, the system modifies its magnetic structure every time through a reorientation of the strongly anisotropic rare-earth moments (i.e. a kind of 'magnetic' Jahn–Teller effect, see [9]). The minimal splitting (near-crossing) occurs when the applied magnetic field fully compensates the exchange field (i.e. same splitting pattern as with CF alone). In this situation, by increasing the distance of quasi-doublet from excited levels, the applied magnetic field tends to give the Ho^{3+} ion an Ising behavior, and hence induces the jumps observed on the isothermal magnetization curves.

4. Phase diagrams and discussion

In our previous calculation [11], only the lower closely lying singlets were considered (fictitious-spin Hamiltonian). Now, we deal with the action of the different interactions on the Ho^{3+} ion described by its ground multiplet J with its 17 levels. To find the energy levels, we have to diagonalize the effective Hamiltonian which simultaneously combines CF, exchange field and applied magnetic field interactions. This is unavoidable, because even when the CF is large, some

low-lying energy levels are so close as to be strongly connected by the Ho–Fe exchange interaction.

In the 2–30 K temperature range and 0–23 T field range, $M_{\mathrm{Fe}} = 5\ \mu_{\mathrm{B}}$ and is temperature and field independent. In fact, it can be considered constant to within 0.3%. This is known from the high-field magnetization data of YIG [31]. These data also show that M_{Fe} is also insensitive to the exchange field coming from the rare-earth sublattices. Then, if the nine CF parameters are known, one can always determine the Ho moment directions given the direction $\mathbf{n}(\theta, \phi)$ of M_{Fe}, under an applied magnetic field $\boldsymbol{H}$ and at a temperature T. The direction $\mathbf{n}(\theta, \phi)$ is the relevant parameter for discussing the stability of the different magnetic phases. The free energy F of $\mathcal{N}$ (Avogadro's number) molecules of $\mathrm{Ho}_x\mathrm{Y}_{3-x}\mathrm{Fe}_5\mathrm{O}_{12}$ can be written:

$$F(\mathbf{n}, \boldsymbol{H}, T) = -\mu_0 \boldsymbol{H} \cdot \boldsymbol{M}_{\mathrm{Fe}} + \frac{x}{6}\left(-\mathcal{N} k_{\mathrm{B}} T \ln \prod_{q=1}^{6} Z_q\right) \quad (2)$$

with $Z_q = \mathrm{Tr}\, \mathrm{e}^{-\beta(\mathcal{H})_q}$ the single-particle canonical partition function for the qth inequivalent site, occupied by one of the noninteracting rare-earth ions. Here Tr stands for the trace and $\beta = (k_{\mathrm{B}} T)^{-1}$ the inverse temperature.

But the Hamiltonian of a rare-earth ion located at the qth site is now given by:

$$(\mathcal{H})_q = (\mathcal{H}_{\mathrm{CF}} + \mathcal{H}_{\mathrm{Zeeman}})_q \quad (3)$$

where $\mathcal{H}_{\mathrm{CF}}$ is the CF interaction as defined by (1), and $\mathcal{H}_{\mathrm{Zeeman}}$ is the interaction with the total effective field $\boldsymbol{H}_{\mathrm{eff}} = \boldsymbol{H} + \boldsymbol{H}_{\mathrm{mol}}$. In order to model the exchange interaction we used the molecular field $\boldsymbol{H}_{\mathrm{mol}} = -n \cdot \boldsymbol{M}_{\mathrm{Fe}}$, treated as a parameter and assumed to behave like a true magnetic field. Here n is the isotropic molecular-field coefficient. We deduced earlier [10] that its value can be taken equal to 2.2 T mol/μ_{B} (i.e. $\boldsymbol{H}_{\mathrm{mol}} = 11$ T). The molecular field is related to the exchange field ($\boldsymbol{H}_{\mathrm{ex}} = 27.5$ T), which acts only on the spin, by the relation $\boldsymbol{H}_{\mathrm{ex}} = (g_J/2(g_J - 1))\boldsymbol{H}_{\mathrm{mol}}$. In addition, by considering it in the iron direction we neglect the Ho^{3+}–Fe^{3+} exchange interaction anisotropy and the iron sublattice anisotropy which is known to be very small in YIG. The effective field $\boldsymbol{H}_{\mathrm{eff}}$ is expressed in the local coordinate system of each site q (q = 1–6). For an ion of the system of Ho^{3+} at qth site, the state space is spanned by the basis states $\{|\Psi_q^i\rangle\}$, eigenvectors of $(\mathcal{H})_q$ with the eigenvalues E_q^i. In the canonical ensemble, the single-particle Boltzmann–Gibbs density operator at equilibrium is:

$$\hat{\mathbf{D}}_q = Z_q^{-1} \mathrm{e}^{-\beta(\mathcal{H})_q}. \quad (4)$$

The magnetic-moment operator of an ion at qth site is defined by:

$$\hat{\boldsymbol{m}}_q = (-g_J \mu_{\mathrm{B}} \hat{\boldsymbol{J}})_q \quad (5)$$

and the magnetic moment is the expectation value of this operator, i.e. we have

$$\boldsymbol{m}_q = \langle \hat{\boldsymbol{m}}_q \rangle = \mathrm{Tr}\, \hat{\mathbf{D}}_q \hat{\boldsymbol{m}}_q = \sum_{i=1}^{17} -g_J \mu_{\mathrm{B}} \left\langle \Psi_q^i \middle| \hat{\boldsymbol{J}} \middle| \Psi_q^i \right\rangle Z_q^{-1} \mathrm{e}^{-\beta E_q^i}. \quad (6)$$

We can therefore consider these q-site magnetic moments as three-component classical vectors. They are expressed in the corresponding local coordinate systems. We convert them into the crystal coordinate system and, for $\mathcal{N}$ molecules, the overall magnetic moment of the mixed holmium–yttrium garnet is given by:

$$\boldsymbol{M} = \boldsymbol{M}_{\mathrm{Fe}} + \boldsymbol{M}_{\mathrm{Ho}} = \boldsymbol{M}_{\mathrm{Fe}} + \frac{x}{6} \sum_{q=1}^{6} \boldsymbol{\mathcal{M}}_q \quad (7)$$

where $\boldsymbol{\mathcal{M}}_q = \mathcal{N} \boldsymbol{m}_q$ is the bulk magnetic moment of the Ho^{3+} ion at the qth site. For comparison with measured magnetization curves, the calculated magnetization of the compound is obtained by finding the projection of (7) on the direction of the applied magnetic field. The procedure for precisely determining the different stable magnetic configurations of the moments and their energies comparison is exactly the same as in our previous work [11]. From the eigenstates and energy levels of the Ho ions in the crystalline and effective fields, we can calculate the magnetic structure of Ho moments and the free energy F relative to the vector $\boldsymbol{M}_{\mathrm{Fe}}$ angles (θ, ϕ), for each given values of the field H and temperature T. Thus, for fixed T and H the equilibrium configurations are given by numerical minimization of F with respect to the $\boldsymbol{M}_{\mathrm{Fe}}$ angles (θ, ϕ). The unique difficulty with numerical calculations of bulk properties could come from the fact that the unit cell contains six rare-earth inequivalent magnetic sites. But this is easily tackled owing to the ability of the Scilab [30] programming language to handle matrices. In the program, we just replace the block relative to the effective-spin Hamiltonian by the block which does the diagonalization of the CF and Zeeman Hamiltonians together, without forgetting to take into account the Hutching and Wolf convention of local axes (see figure 1) adopted in CF calculations. It is worth noting that in constructing the calculated phase diagram corresponding to effective-spin Hamiltonian, we took the parameters found in [11] and the local z-axis along the ⟨001⟩ direction, as usually adopted within spin-Hamiltonian formalism. In all cases lowest minima were determined unambiguously.

At zero field, the number of phases is none other than the eight ferrimagnetic domains where the rare-earth magnetization $\boldsymbol{M}_{\mathrm{Ho}}$ is tied along the various equivalent easy directions ⟨111⟩. When the applied field and $\boldsymbol{M}_{\mathrm{Fe}}$ are parallel to a high-symmetry direction, the non-collinear structure of rare-earth moments adopts the same symmetry axis and the phase is called coaxial. Since the change of orientation of $\boldsymbol{M}_{\mathrm{Fe}}$ is accompanied by a change of the magnitudes of the magnetic moments of the Ho^{3+} ions at the different sites, $\boldsymbol{M}_{\mathrm{Ho}}$ is not parallel to ⟨111⟩ directions outside coaxial phases. But one can always identify each phase by the appropriate ⟨111⟩ orientation that $\boldsymbol{M}_{\mathrm{Fe}}$ (and then $\boldsymbol{M}_{\mathrm{Ho}}$) would have in zero applied field (of course, we assume that the concerned phase is still being favored when the field is removed). The labeling may be continued unambiguously as earlier [11]. For peculiar direction $\boldsymbol{u}$ of the applied magnetic field H, several of these ⟨111⟩ domains can have the same projection on H, and so they are equivalent and constitute the same degenerate phase.

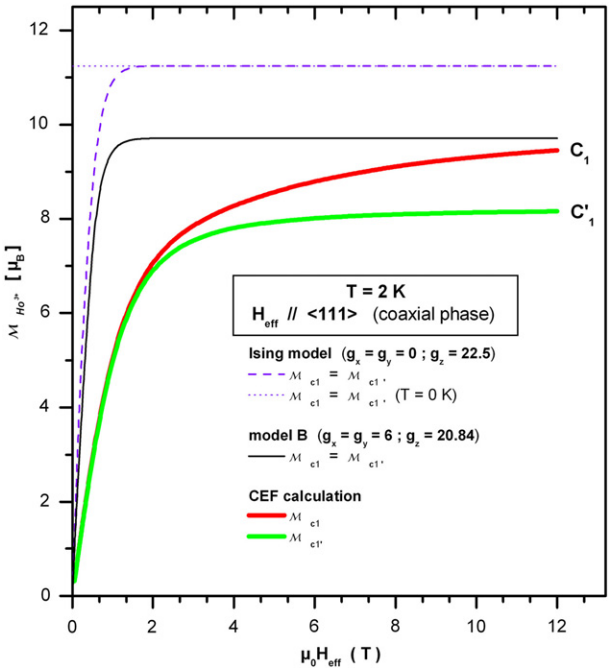

Figure 7. Variation of the Ho moment for the different models in coaxial phase (i.e. $\boldsymbol{H}_{\rm eff} \parallel [111]$) as a function of applied field: $T = 2$ K.

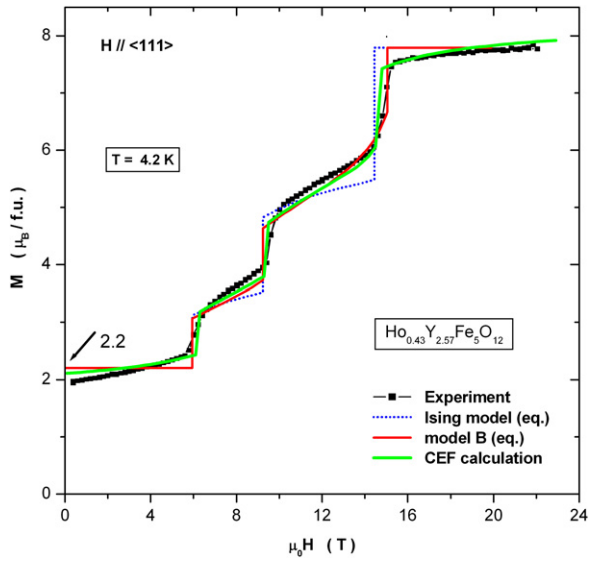

Figure 8. Experimental magnetization curve compared with those calculated using the different models: $\boldsymbol{H} \parallel [111]$ and $T = 4.2$ K.

From the number $n_p(\boldsymbol{u})$ of inequivalent phases ($P^i_{\boldsymbol{u}}$, $i = 1$ to n_p) we deduce the number of magnetization jumps which is obviously equal to $n_p(\boldsymbol{u}) - 1$. For $\boldsymbol{H} \parallel [111]$ (below T^*), there are four phases, namely, in order of appearance when the field increases, $P^1_{111} = \{[\bar{1}\bar{1}\bar{1}]\}$, $P^2_{111} = \{[1\bar{1}\bar{1}], [\bar{1}1\bar{1}], [\bar{1}\bar{1}1]\}$, $P^3_{111} = \{[11\bar{1}], [1\bar{1}1], [\bar{1}11]\}$ and $P^4_{111} = \{[111]\}$, leading to three phase transitions between them. This is the successive reorientation of the moments of Ho sublattices from the configuration with the resultant moment $\boldsymbol{M}_{\rm Ho} \parallel [\bar{1}\bar{1}\bar{1}]$ to the saturated one with $\boldsymbol{M}_{\rm Ho} \parallel [111]$. For $\boldsymbol{H} \parallel [110]$, there are two transitions between the three phases $P^1_{110} = \{[\bar{1}\bar{1}1], [\bar{1}1\bar{1}]\}$, $P^2_{110} = \{[1\bar{1}\bar{1}], [\bar{1}1\bar{1}], [1\bar{1}1], [\bar{1}11]\}$ and $P^3_{110} = \{[11\bar{1}], [111]\}$.

Figures 5 and 6 give a comparison between experimental phase diagrams for ⟨110⟩ and ⟨111⟩ directions, and those calculated in the frame of the effective-spin Hamiltonian model (uniaxial model) and in the frame of the CF model. It may be seen that the phase diagrams calculated from the CF levels agree very well with the experimental ones. In particular, the critical temperature T^*, which equals 18.9 K for the two directions. Considering the CF levels has induced a diminution of the rare-earth moments $\mathcal{M}_{\rm Ho}$ with increasing temperature, which caused lowering of critical temperature. This diminution is all the more pronounced as these moments decrease significantly when the applied field increases. The variation of moments versus the effective field is shown in figure 7 for the different models: Ising, uniaxial (model B) and CF (CEF).

In figure 8, we compare the isothermal magnetization curves, calculated in the frame of the CF and the other models, with the measured magnetization curve at $T = 4.2$ K. It can be seen that the curve calculated from CF levels is in excellent agreement with the experimental one. Now the magnetization jumps are accurately calculated for the three transitions. We have to note also the correct change of the magnetization with the field in the initial coaxial phase, contrasting with the 'absolute rigidity' of the umbrella structure in the fictitious-spin models where the moment magnitude is constant. The non-collinear structure is a 'double-umbrella' which varies with the field right at the start. In this phase, the field can only open it and reduce the magnitude of the moments. When the applied field increases from zero up to first transition field, the moments at C_1 and C'_1 sites change from 9.39 μ_B and 8.15 μ_B to 8.58 μ_B and 7.94 μ_B, respectively. The angles for their part change from 23.46° and 53.45° to 31.06° and 54.14°, respectively. The weak increase of the magnetization in this phase and the smallness of the initial susceptibility fix an upper limit for these two same-direction processes and give evidence of an appreciable rigidity of this 'double-umbrella' magnetic structure, i.e. the local anisotropy of the Ho ion.

Moreover, the calculated free energy indicates, as expected, that ⟨111⟩ is the direction of easy magnetization. At $T = 1.5$ K, the computed anisotropy energy is $\Delta F = F_{[111]} - F_{[001]} = -7.6$ cm^{-1}/Ho^{3+}. In our case $H_{\rm mol} = 11$ T, but if we take $H_{\rm mol} = 9.4$ T as in [14], we found $\Delta F = -6.4$ cm^{-1}/Ho^{3+}, to compare with $\Delta F = -6.6$ cm^{-1}/Ho^{3+} [14] and with magnetocrystalline measurements which give $\Delta F = -6.9$ cm^{-1}/Ho^{3+} [32]. Contrary to the ESH model [11], the calculation now accounts for a 'double-umbrella' magnetic structure, since we found the following results at $T = 4.2$ K: $\mathcal{M}_{C'_1} = 8.15\ \mu_B$, $\theta_{C'_1} = 53.45°$ for the site C'_1, and $\mathcal{M}_{C_1} = 9.39\ \mu_B$, $\theta_{C_1} = 23.46°$ for the site C_1. These values are in good agreement with Nekvasil's calculation and RMN measurements [14], but disagree with the neutron spectra refinements of Guillot *et al* [13], where the moment $\mathcal{M}_{C_1}$ was found far from ⟨111⟩ and outside D_2 symmetry planes. As already noticed by Nekvasil [14], this disagreement is probably due to the confusion between C_i- and C'_i- sites during refinements in [13]. From our measured

magnetization curve at $T = 4.2$ K (figure 8), we deduce a value for the Ho^{3+} mean magnetic moment of $6.86 \pm 0.21\ \mu_B$, while the calculated value is $6.73\ \mu_B$.

5. Conclusion

We constructed the magnetic phase diagram of the $Ho_{0.43}Y_{2.57}Fe_5O_{12}$ garnet by magnetization measurements under high static magnetic fields on oriented single crystals in the low temperature range 2–30 K. We have been able to show that, starting from what is known about the CF effects on Ho^{3+} in these diluted garnets, an excellent agreement of calculated magnetization curves and phase diagrams can be obtained if one use some experimentally interpolated parameters and a simple mean-field approximation for the Ho–Fe interaction treated as an effective field. The CF approach has the great merit of involving realistic parameters, contrary to the fictitious-spin Hamiltonian which is not exempt from criticism for rare-earth ions, especially for an even-electron system such Ho^{3+}. Although these CF parameters can be further improved, this study is already a good validation for them.

Acknowledgments

Fruitful discussions with Professor A Zvezdin are gratefully acknowledged. This work would not have been possible without the garnet crystals grown by Dr B Mill' and provided by Dr A Markosyan. We express our warm thanks to F Givord for her interest in this study and her help in the CF calculations. We should also like to thank A Richard for technical assistance during the high-field measurements at the Grenoble High Magnetic Field Laboratory (GHMFL is 'laboratoire associé à l'Université Joseph Fourrier–Grenoble'). AB acknowledges the support of the French–Algerian grant program through BFA no 2002652.

References

[1] Gapeev A K, Levitin R Z, Markosyan A S, Mill' B V and Perakalina T 1975 *Sov. Phys.—JETP* **40** 117
[2] Levitin R Z, Ponomarev B K and Popov Y F 1971 *Sov. Phys.—JETP* **32** 1056
[3] Demidov V G and Levitin R Z 1977 *Sov. Phys.—JETP* **45** 581
[4] Silant'ev V I, Popov A I, Levitin R Z and Zvezdin A K 1980 *Sov. Phys.—JETP* **51** 323
[5] Babushkin G, Zvezdin A K, Levitin R Z, Popov A I and Silant'ev V I 1981 *Sov. Phys.—JETP* **53** 1015
[6] Lagutin A S 1991 *Sov. Phys.—JETP* **72** 189
[7] Lagutin A S 1992 *Sov. Phys.—JETP* **75** 138
[8] Lagutin A S 1994 *Physica* B **201** 63
[9] Zvezdin A K, Mukhin A A and Popov A I 1977 *Sov. Phys.—JETP* **45** 573
[10] Bouguerra A, Khène S and Fillion G 2004 *Phys. Status Solidi* c **1** 1683
[11] Bouguerra A, Khène S, de Brion S, Chouteau G and Fillion G 2005 *J. Phys.: Condens. Matter* **17** 241–8
[12] Herpin A, Koehler W and Meriel P 1960 *C. R. Acad. Sci. Paris* **251** 1359
[13] Guillot M, Tchéou F, Marchand A and Feldmann P 1984 *Z. Phys.* **56** 29
[14] Englich J, Lütgmeier H, Pieper M W, Nekvasil V and Novák P 1985 *Solid State Commun.* **56** 825
[15] Nekvasil V 1979 *Phys. Status Solidi* b **94** K41
[16] Racah G 1942 *Phys. Rev.* **62** 438
[17] Racah G 1943 *Phys. Rev.* **63** 367
[18] Wybourne B G 1965 *Spectroscopic Properties of Rare Earths* (New York: Interscience)
[19] Newman D J and Ng B (ed) 2000 *Crystal Field Handbook* (Cambridge: Cambridge University Press)
[20] Walter U 1984 *J. Phys. Chem. Solids* **45** 401
[21] Leech J W and Newman D J 1969 *How to Use Groups* (London: Methuen)
[22] Grünberg P, Hüfner S, Orlich E and Schmitt J 1969 *Phys. Rev.* **184** 285
[23] Orlich E, Hüfner S and Grünberg P 1970 *Z. Phys.* **231** 144
[24] Hutchings M T and Wolf W P 1964 *J. Chem. Phys.* **41** 617
[25] Dieke G H and Crosswhite H M 1963 *Appl. Opt.* **2** 675
[26] Osborn R, Lovesey S W, Taylor A D and Balcar E 1991 *Handbook on the Physics and Chemistry of Rare Earths* vol 14, ed K A Gschneider and L Eyring (Amsterdam: Elsevier) p 21
[27] Johnson L F, Dillon J F Jr and Remeika J P 1970 *Phys. Rev.* B **1** 1935
[28] Onn D G, Meyer H and Remeika J P 1967 *Phys. Rev.* **156** 663
[29] Bouguerra A, Fillion G, Givord F and Murani A 2008 at press
[30] Gomez C 1999 *Engineering and Scientific Computing with Scilab* (*Claude Gomez/INRIA-Rocquencourt, France*) (Boston, MA: Birkhaüser) (ISBN 0-8176-4009-6)
[31] Pauthenet R 1982 *J. Appl. Phys.* **53** 8187
[32] Pearson R F and Cooper R W 1962 *J. Phys. Soc. Japan* **17** 369